Nanoscale Advances

ROYAL SOCIETY OF CHEMISTRY

PAPER

View Article Online
View Journal | View Issue

Cite this: *Nanoscale Adv.*, 2023, **5**, 4536

Targeted and efficient delivery of rifampicin to macrophages involved in non-tuberculous mycobacterial infection *via* mannosylated solid lipid nanoparticles

Jayoung Chae,[ab] Seung Hyun Kang,[c] Jiwon Kim,[a] Yonghyun Choi,*[abc] Shin Hyuk Kang*[c] and Jonghoon Choi *[ab]

Non-tuberculous mycobacterial infections are representative difficult-to-cure lung diseases with high incidence. Conventional treatments have several limitations such as negative side effects and increased drug resistance due to long-term administration. To overcome these limitations, there is a growing need for more stable drug delivery systems. Among the various drug delivery platforms developed thus far, solid lipid nanoparticles can be effectively loaded with hydrophobic substances and their physicochemical properties can be easily manipulated through surface modification, which makes them highly suitable drug delivery materials. Recent studies have reported the successful development of nanoparticles capable of selectively delivering drugs by targeting lectin-like receptors overexpressed on the surface of immune cells. Among these lectin-like receptors, the mannose receptor is a promising target because it is expressed on the surface of macrophages and is involved in immune activity. This study sought to synthesize rifampicin-loaded mannose surface-modified solid lipid nanoparticles (Man-RIF SLNs). The Man-RIF SLN synthesis process was first optimized, after which the characteristics of the synthesized particles were analyzed using dynamic light scattering (DLS), nanoparticle tracking analysis (NTA), and transmission electron microscopy (TEM). The surface modification with mannose was confirmed through FT-IR analysis. More importantly, the synthesized Man-RIF SLNs exhibited antibacterial and anti-biofilm properties against *Mycobacterium intracellulare*, a causative agent of non-tuberculous lung disease. Therefore, this study demonstrated that mannose receptor-targeted rifampicin delivery through solid lipid nanoparticles can be effectively applied to the treatment of non-tuberculous lung disease. Moreover, Man-RIF SLNs could also be used for the targeted delivery of drugs to several types of carcinoma cells or immune cells, as well as to treat lung diseases.

Received 11th May 2023
Accepted 25th July 2023

DOI: 10.1039/d3na00320e

rsc.li/nanoscale-advances

Introduction

Infectious mycobacterial lung diseases are among the leading threats to lung health worldwide and are notoriously difficult to treat. The two main causative agents of mycobacterial lung infections are *Mycobacterium tuberculosis* (TB) and non-tuberculous mycobacteria (NTM). However, although the incidence of TB has been slowly declining over the past few decades, the global incidence of NTM lung disease continues to increase at a rapid pace.[1] *Mycobacterium avium* complex (MAC) species, particularly *M. avium* and *M. intracellulare*, are the most common cause of NTM lung infections worldwide and are among the most difficult species to treat. Unlike *M. tuberculosis*, there is no evidence of human-to-human transmission of MAC species. Instead, MAC species are common organisms found in urban water sources, soil, and dirt, and can cause serious lung disease in patients with underlying conditions such as bronchiectasis, chronic obstructive pulmonary disease, and cystic fibrosis.[2,3] MAC infections are particularly common in patients with severe immunodeficiency, such as those with advanced HIV infection and malignancy, as well as those with a history of immunosuppressive therapy such as anti-tumor necrosis factor-α (TNF-α).[4,5] Although less common, NTM lung disease can also occur in healthy people without genetic or immunologic predispositions.[6] Currently, the treatment of NTM infections relies heavily on TB drugs, as the mechanism of infection is similar. Rifampicin is a broad-spectrum antibiotic that is commonly used as the main treatment against TB and is often used in combination with other first-line antituberculosis

[a]*School of Integrative Engineering, Chung-Ang University, Seoul 06974, Republic of Korea. E-mail: dydgus5057@cau.ac.kr; nanomed@cau.ac.kr*

[b]*Feynman Institute of Technology, Nanomedicine Corporation, Seoul 06974, Republic of Korea*

[c]*Departments of Plastic and Reconstructive Surgery, Chung-Ang University Hospital, Chung-Ang University College of Medicine, Seoul 06973, Republic of Korea. E-mail: kangshinhyeok@cau.ac.kr*

drugs. MAC infection is also treated with chemotherapy using these antituberculosis drugs, particularly macrolides and a combination of rifampicin, azithromycin, and three other drugs. However, current NTM treatments rely on a multi-drug regimen that includes these antituberculosis drugs for at least 12 months.[7,8] Prolonged drug treatment, as well as frequent check-ups or hospitalization, can often result in a significant financial burden for patients. Treatment is also often discontinued due to long treatment periods, slow progress, and side effects associated with oral and parenteral administration of the drug, such as gastrointestinal distress, skin rashes, renal failure, and liver toxicity.[1,9,10] Among other challenges, the rise of drug resistance in the treatment of mycobacteria is one of the major obstacles to curing this disease.[11,12] Therefore, strategies to deliver existing drugs more efficiently are needed to shorten treatment duration, reduce drug resistance, and improve patient adherence.

To overcome the limitations of conventional chemotherapeutic regimens, including anti-TB drugs, there is an emerging need for the development of effective drug delivery systems such as polymers, lipid nanoparticles and magnetic nanoparticles.[13–15] The effectiveness of a drug *in vivo* does not depend solely on its physicochemical properties but also on the carrier system that can enhance its bioavailability.[13] In turn, this can maximize drug efficiency, as well as patient safety and adherence.[16] Lipid-based nanoparticle delivery systems have good biocompatibility and can increase the activity of drugs by increasing their availability. These delivery systems have also been extensively studied as carriers of various drugs (*e.g.*, anticancer drugs) because targeted delivery can minimize unnecessary drug exposure, thereby minimizing side effects.[17–20] The lipid core of solid lipid nanoparticles (SLNs) plays an important role in modulating the release pattern of drugs and can improve their bioavailability by protecting the loaded drug from chemical, optical, and enzymatic degradation.[16] Additionally, SLNs have received widespread attention as a drug delivery vehicle to replace liposomes and polymeric nanoparticles because they can improve the sustained release, targeting ability, physical stability, and drug absorption efficiency of the loaded drug, in addition to overcoming the shortcomings of other colloidal nanoparticles such as acute and chronic toxicity.[17,21,22]

Similar to TB, NTM also infiltrates alveolar macrophages in the lungs and causes infection by inhibiting phagosome/lysosome formation. Therefore, a targeted drug delivery system specific to alveolar macrophages could provide an effective means to eliminate bacterial cells.[23,24] Alveolar macrophages express lectin receptors on their surface, which recognize glycoconjugates with a high binding affinity.[25] Glycotargeting is achieved through the interaction of ligands such as mannose, galactose, and lactose with specific receptors expressed on the cell surface. The binding of cell membrane lectin receptors to specific carbohydrate subunits can lead to receptor-mediated internalization.[26,27] Particularly, the combination of mannose with various drug carriers is being actively studied.[28,29] Previous studies have reported that mannose-modified nanoparticles can be used to target macrophages and dendritic cells to activate the immune response with high macrophage uptake rates, good activity, and reduced side effects.[30] These results suggest that mannose is preferentially and selectively taken up by alveolar macrophages, and therefore polysaccharide-nanoparticle formulations can be utilized as effective agents for targeted drug delivery to alveolar tissue.[31]

In this study, mannose surface-modified solid lipid nanoparticles were used to more effectively deliver rifampicin, which is commonly used as a therapeutic agent for the treatment of non-tuberculous lung disease. By incorporating the hydrophobic drug rifampicin into solid lipid nanoparticles, we created a drug delivery system that could prevent unnecessary drug degradation by delivering the drug stably and directly to its target tissue. The surface of the solid lipid nanoparticles was modified with mannose to target the mannose receptor on the surface of *Mycobacterium intracellulare* (*M.i.*)-infected macrophages. By doing so, we aimed to improve the targeted delivery of drugs (Scheme 1). To achieve this, solid lipid nanoparticles loaded with rifampicin were first synthesized, after which the surface of the particles was modified using mannose. The synthesized particles were characterized to confirm their size and mannose coating. Next, we confirmed the antibacterial and anti-biofilm effects of Man-RIF SLNs on *M.i.*, meaning that the developed drug delivery system could be used to enhance the therapeutic efficiency of current non-tuberculous lung disease treatments. Collectively, our findings demonstrated that the Man-RIF SLN is an effective formulation to improve the therapeutic efficacy of existing drugs by increasing their stability and reducing side effects.

Materials and methods

Materials

Glycerol tripalmitate was purchased from Thermo Fisher Scientific (MA, USA). Rifampicin (RIF) was purchased from Tokyo Chemical Industry (TCI, Japan). Octadecylamine (SA), D-(+)-mannose, Tween 80, SpectraPor® 12–14 kDa dialysis membranes, Triton X-100, phorbol myristate acetate (PMA), Middlebrook 7H9 broth base, Middlebrook 7H10 agar base, oleic acid, bovine serum albumin, bovine liver catalase, and glycerol were obtained from Sigma-Aldrich (St. Louis, MO, USA). Dextrose and sodium chloride were purchased from Duksan general science (Korea). 3-(4,5-Dimethylthiazol-2-yl)-2,5-diphenyltetrazolium bromide (MTT) was purchased from VWR Life Sciences (Radnor, PA, USA). Interleukin-4 (IL-4) and interleukin-13 (IL-13) used for macrophage differentiation and polarization were obtained from PeproTech (Cranbury, NJ, USA).

Methods

Preparation of rifampicin-loaded solid lipid nanoparticles (RIF-SLNs)

Rifampicin-loaded SLNs and bare SLNs were prepared through a combination of high-shear homogenization and hot sonication methods. Briefly, glycerol tripalmitate and rifampicin as the lipid phase were heated to 80 °C until the lipid was completely dissolved. The aqueous phase, which was prepared

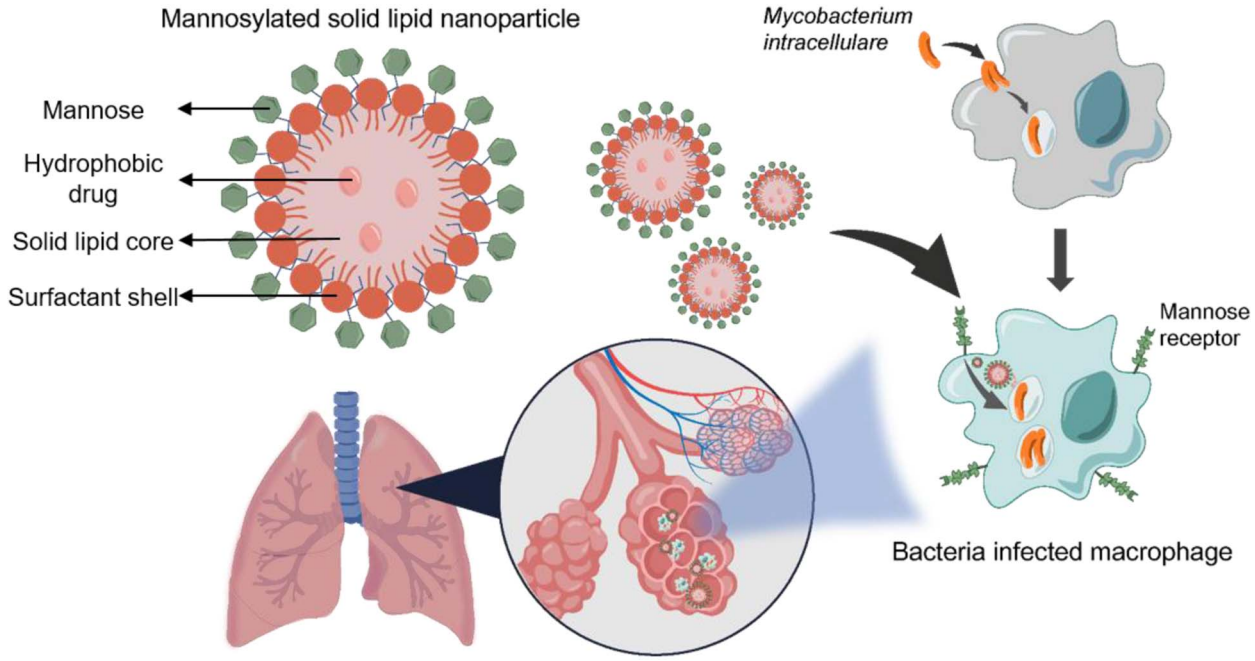

Scheme 1 Targeted treatment of *M. intracellulare* (*M.i.*) infected macrophages by delivering rifampin with mannosylated solid lipid nanoparticles (Man-RIF SLN). *M.i.* causes infection inside the macrophage and the infected macrophages express the mannose receptor on the surface. By targeting this receptor using Man-RIF SLNs, the delivery efficiency of the drug can be greatly increased while minimizing side effects.

by dissolving a surfactant (Tween 80) in double-deionized water, was also heated to the same temperature. Next, the aqueous phase was mixed with the lipid phase to obtain an emulsion by homogenization at 12 400 rpm for 2 min with a T 10 basic ULTRA-TURRAX® homogenizer (IKA, Germany). The emulsion was then sonicated using a VCX-500 & VCS-750 ultrasonic processor (Sonics, USA) at 20% amplitude for 5 min, followed by homogenization again under the same conditions described above. The final preparation was allowed to cool at room temperature and kept refrigerated in an amber glass vial.

Mannose functionalization on the surface of the SLNs

Mannose functionalization was conducted *via* the ring-opening reaction of mannose, in which an aldehyde group of mannose reacts with a free amine group provided by stearylamine (SA) in sodium acetate buffer (pH 4.0). SA was added in the lipid phase at a 4% (w/w) ratio, after which all subsequent steps were performed exactly as described above. A D-mannose solution (50 mM) in acetate buffer (pH 4.0) was added to the RIF-SLNs, after which the mixture was left in agitation with gentle magnetic stirring at room temperature for 48 h. Mannosylated SLNs were subjected to extensive dialysis (MWCO 12–14 kDa) against double distilled water for 20 min to remove unconjugated mannose.

Characterization of the formulations

Particle size and zeta potential

The size and zeta potential were measured using a Zetasizer Pro (Malvern, UK). The particle concentration was measured using a NanoSight LM10 nanoparticle tracking analysis instrument (Malvern, UK). Before measurement, the SLN suspensions were diluted in deionized water (DW) to suitable concentrations to obtain better focusing positions and attenuation.

Transmission electron microscopy (TEM) analysis

The shape and morphology of nanoparticles were observed *via* field emission transmission electron microscopy (FE-TEM) analysis. The samples were prepared by placing a drop of nanoparticle suspension on a carbon-coated nickel-mesh grid. Images were obtained using a JEM-F200 transmission electron microscope (JEOL Ltd, Japan) with an accelerating voltage of 80 kV.

Fourier transform infrared spectrum (FT-IR) analysis

Lyophilized formulations were analyzed *via* Fourier transform infrared spectroscopy (FT-IR) to confirm that the nanoparticles had been successfully coated with mannose. The freeze-dried bare SLNs, RIF-SLNs, Man-RIF SLNs, and mannose were evaluated using an FT-IR spectrophotometer (ALPHA II, Germany). The samples were transferred directly to the attenuated total reflectance compartment, and the collected spectra were analyzed between the 4000 and 400 cm^{-1} region, submitted to baseline correction, and area-normalized for further comparison.

In vitro drug release study

An *in vitro* drug release study was performed using the dialysis bag method. A dialysis membrane bag (12–14 kDa molecular

weight cutoff; Spectrum™ Spectra/Por™ 3 RC Dialysis Membrane Tubing, USA) was filled with a solution containing the same concentration of Man-RIF SLN suspension and free rifampicin, and 10 mL 50% methanol buffer was used as an external buffer. The dialysis samples were then incubated on an orbital shaker at 37 °C and 200 μL of sample was collected at different time intervals for approximately 24 h. An equal volume of new buffer was added to the external buffer to maintain sink conditions. The rifampicin concentration in the collected samples was measured at a wavelength of 470 nm using a microplate reader (BioTek/Agilent, USA).

Physical stability study

The synthesized particles were refrigerated and stored at 4 °C in an amber glass vial. To confirm the physical stability of the particles, their size, polydispersity index (PDI), and zeta potential were measured immediately after synthesis and after 9 months *via* dynamic light scattering (DLS) analysis. For the DLS measurements, the nanoparticle solution was diluted with DW, and all measurements were conducted in triplicate.

Cell culture

Immortalized human monocytes (THP-1) were obtained from the American Type Culture Collection (Rockville, MD, USA). The THP-1 cell line was maintained in suspension in T25 flasks with ATCC-modified RPMI medium (RPMI, Gibco). The culture media was supplemented with 10% fetal bovine serum (FBS, Gibco) and 1% antibiotic–antimycotic (A/A, Hyclone) and then incubated at 37 °C under 5% CO_2 and 90–95% humidity.

In vitro analysis of cytotoxicity on macrophages

The MTT assay was performed to confirm the cytotoxicity of bare SLNs, RIF-SLNs, Man-RIF SLNs, and free rifampicin on macrophages. THP-1 cells were seeded onto a 96-well plate at a 5×10^4 cells per well density and treated with fresh RPMI culture medium containing 100 ng mL^{-1} of PMA for 24 h to allow for cell differentiation. After incubation, the cells were washed with DPBS and M2 macrophages were prepared by cell polarization with interleukin-4 (IL-4) and interleukin-13 (IL-13) for 24 h. The cells were then treated with SLNs, RIF-SLNs, Man-RIF SLNs, and free rifampicin in fresh media at a 50 μg mL^{-1} concentration for 24 h at 37 °C. Next, the cells were incubated with 2 mg mL^{-1} MTT (Thiazolyl blue tetrazolium blue) solution for 1 h to induce formazan formation. After removing the MTT solution, the formazan crystals were dissolved by adding the same volume of DMSO. The cytotoxic effects of each of the treatments were compared by quantifying the formazan concentration at a wavelength of 570 nm using a microplate reader.

Bacterial growth conditions

M. intracellulare (*M.i.*, KCCM 42852) cells were obtained from the Korean Culture Center of Microorganisms (Seoul, Korea). *M.i.* were grown in Middlebrook 7H9 broth with 0.2% glycerol and ADC enrichment (Bovine Serum Albumin, Dextrose, Catalase) or on Middlebrook 7H10 agar with 0.5% glycerol and OADC enrichment (oleic acid, bovine serum albumin, dextrose, catalase, and sodium chloride). The bacteria were harvested at the exponential growth phase at 37 °C. All *M.i.* cultures were performed in BSL2 security cabinets.

Evaluation of the anti-biofilm effects of Man-RIF SLNs on *M.i*

The crystal violet assay was performed on *M.i.* to confirm the anti-biofilm effect of Man-RIF SLNs. RIF-SLNs, Man-RIF SLNs, and free rifampicin were diluted with DPBS at a concentration of 100 μg mL^{-1}, and 100 μL of sample was added to the wells of a 96-well plate. DPBS was used as a negative control and 1% antibiotic–antimycotic (A/A) was used as a positive control. Next, 100 μL of bacteria culture was added to each well at a 1×10^6 CFU mL^{-1} density and incubated for 24 h. After incubation, the bacteria outside the biofilm were removed through DPBS washing, after which 200 μL of 99.9% methanol was added for fixation followed by an additional 20 min of incubation. The plate was then completely dried at room temperature for 30 min after removing the supernatant, and 200 μL of 0.1% crystal violet solution was added to stain the biofilm for 10 min. For biofilm quantification, crystal violet was dissolved in 70% ethanol after DPBS washing to remove the unreacted solution. Finally, the samples were measured at a 590 nm wavelength using a microplate reader.

Antibacterial test on *M.i.* cells

The antibacterial effect of Man-RIF SLNs against *M.i.* bacterial cells was evaluated through a colony-forming unit (CFU) assay. *M.i.* cells were seeded onto a 96-well plate at a density of 1×10^6 bacteria per well with 7H9 broth media. Each well was then treated with SLNs, RIF-SLNs, Man-RIF SLNs, and rifampicin at a concentration of 100 μg mL^{-1} for 24 h at 37 °C. After incubation, the bacteria were diluted to an appropriate concentration, and 100 μL of the diluted solution was spread onto 7H10 agar with ODAC enrichment plates. The plates were incubated for 4 days at 37 °C and the total number of colonies was then counted. DPBS was used as a negative control and 1% antibiotic–antimycotic was used as a positive control.

Antibacterial effects of Man-RIF SLNs on *M.i.* inside macrophages

THP-1 cells were seeded onto 6-well plates at a 1×10^6 cells per well density with fresh RPMI culture medium containing 100 ng mL^{-1} of PMA for 24 h to allow for cell differentiation. Afterward, the differentiated THP-1 cells were washed with PBS and infected with *M.i.* (10 bacteria : 1 cell ratio) for 3 h. Next, the cells were washed twice with PBS and incubated with fresh RPMI without A/A in the presence of bare SLNs, RIF-SLNs, and Man-RIF SLNs at a 100 μg mL^{-1} concentration for 48 h. After incubation, the cells were washed twice with warm PBS and lysed with 0.05% Triton X-100 in PBS. The cells were then diluted with DW and 100 μL aliquots were spread on 7H10 agar with ODAC enrichment plates. Finally, the plates were incubated for 5 days at 37 °C and the bacterial colonies were counted.

Statistical analysis

All analyses, including data processing and graph generation, were conducted using the OriginPro 2015 software (OriginLab, USA) and GraphPad Prism version 7 for Windows (GraphPad Software, USA). Statistical analyses were performed by one-way ANOVA test and Tukey's multiple comparisons *post hoc* test using GraphPad Prism. Each experiment was performed in duplicate and standard deviations were indicated in all graphs using error bars. Statistical significance was set at $P < 0.05$. All significant values in the figures are indicated as follows: $^{*}P < 0.10$, $^{**}P < 0.01$, $^{***}P < 0.001$, and $^{****}P < 0.0001$ *vs.* the control.

Results and discussion

Preparation and characterization of Man-RIF SLNs

To improve the cellular uptake and drug stability of rifampicin, which is a widely used anti-TB drug, Man-RIF SLNs were synthesized through mannose coating after drug incorporation into SLNs. The average size and zeta potential of the synthesized bare SLNs, RIF-SLNs, and Man-RIF SLNs were measured using DLS. The average size of bare SLNs was 205.6 ± 5.3 nm, whereas that of the RIF-SLNs and Man-RIF SLNs was 195.7 ± 6.2 and 217.3 ± 5.4 nm, respectively (Fig. 1A). The zeta potentials of the bare SLNs and RIF-SLNs were −15.2 ± 0.53 mV and −21.8 ± 0.71 mV, respectively, indicating that both particles were negatively charged. In contrast, the Man-RIF SLNs were positively charged (+40.2 ± 0.16 mV) due to the stearylamine added for mannose functionalization (Fig. 1B). Particle concentrations were measured using NTA and our results indicated that there were 8.66×10^{11} particles mL^{-1} for bare SLNs, 4.3×10^{12} particles mL^{-1} for RIF-SLNs, and 4.80×10^{12} particles mL^{-1} for Man-RIF SLNs. To characterize the size and morphology of the Man-RIF SLNs, images of the particles were observed using a transmission electron microscope (TEM). The TEM images confirmed that the synthesized Man-RIF SLNs were nearly spherical in shape and the average size of the particles was approximately 200 nm, which was similar to the results measured by DLS (Fig. 1C). Furthermore, the presence of rifampicin in the synthesized particles was confirmed by measuring the absorbance characteristics of the particles using a microplate reader. As shown in Fig. 1D, no characteristic absorbance peaks were observed for the drug-free Bare SLNs, whereas characteristic peaks of rifampicin were observed for the RIF-SLNs at approximately 340 and 470 nm, thus confirming that rifampicin was loaded within the SLNs.

Mannose functionalization and *in vitro* release study

FT-IR measurements were performed to confirm that the surface of the Man-RIF SLNs had been successfully functionalized with mannose. First, bare SLNs, RIF-SLNs, and Man-RIF SLNs (500 μL of each) were freeze dried for 24 h to prepare the samples, after which the spectra of D-(+)-mannose and the three samples were measured and compared (Fig. 2A). The results of our FT-IR analyses demonstrated the absence of mannose characteristic peaks in the bare SLNs and RIF-SLNs. In

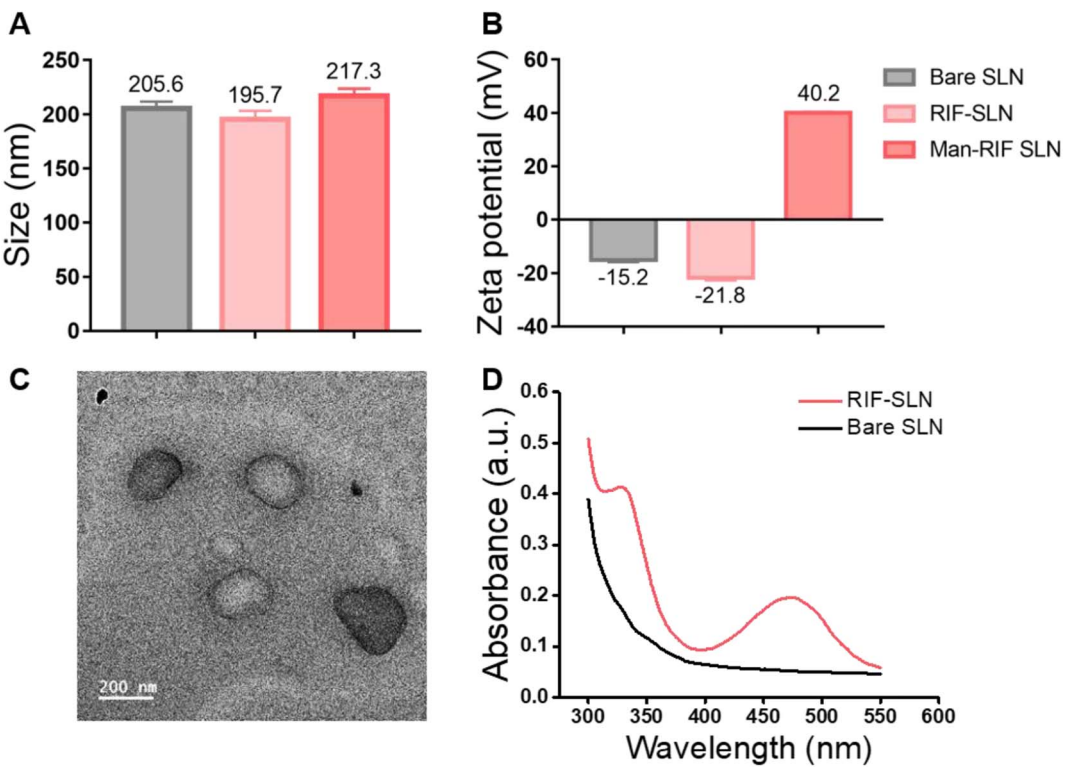

Fig. 1 Characterization of bare SLNs, RIF-SLNs, and Man-RIF SLNs. (A) Particle size and (B) zeta potential of the particle surface. The sizes were similar and the zeta potential changed from a negative to a positive charge in the Man-RIF SLNs. (C) TEM image of Man-RIF SLNs. (D) Absorbance of Man-RIF SLNs.

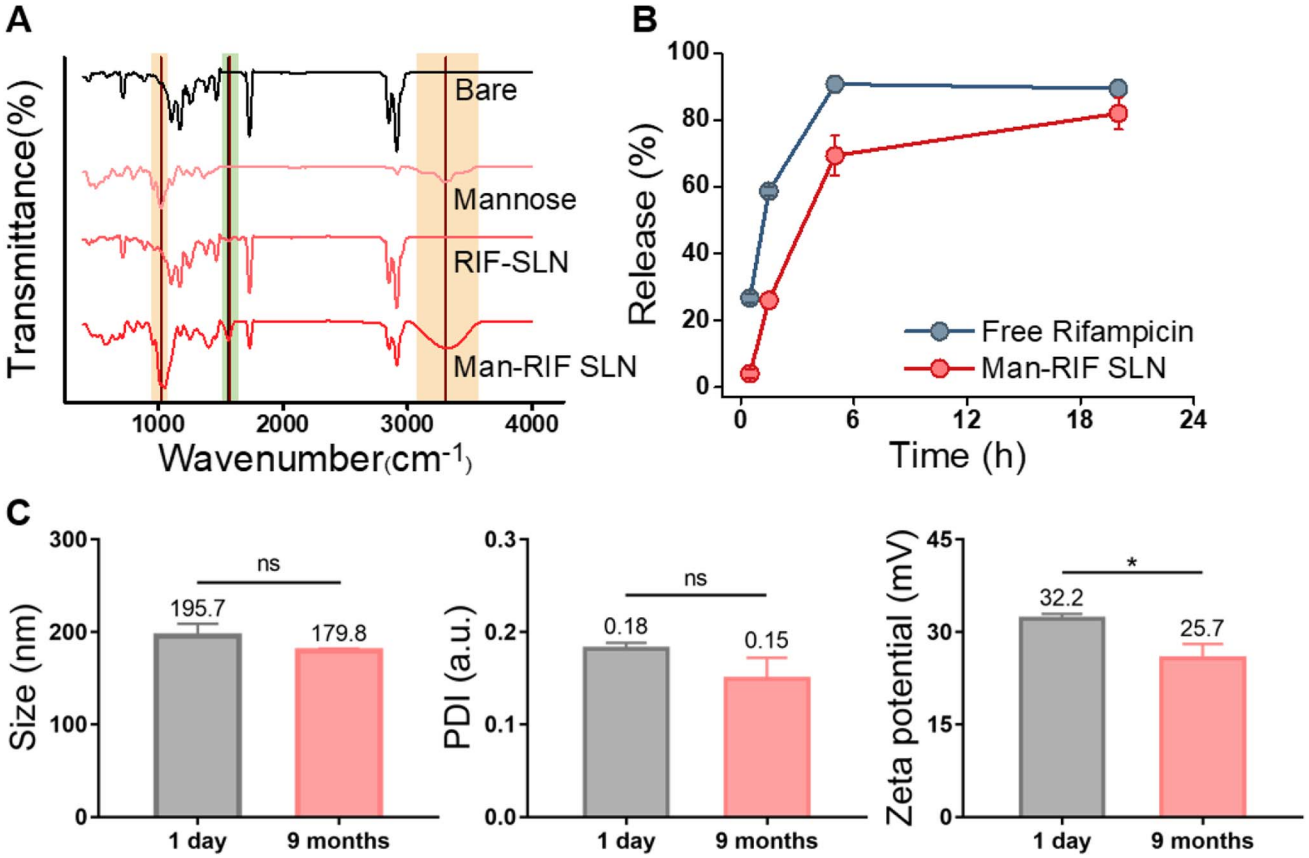

Fig. 2 (A) FT-IR spectra obtained from bare SLNs, RIF-SLNs, Man-RIF SLNs, and mannose to confirm the mannose functionalization of Man-RIF SLNs. (B) Rifampicin release rates from Man-RIF SLN compared to free rifampicin. (C) Physical stability test of Man-RIF SLNs (size, PDI, and zeta potential). Non-significant values are represented as "ns"; *p < 0.0332, **p < 0.0021, ***p < 0.0002, ****p < 0.0001 *vs.* control.

contrast, the Man-RIF SLNs exhibited characteristic mannose peaks at 1021 cm^{-1} and 3300 cm^{-1}. Mannose surface modification was achieved *via* the mannose ring-opening reaction, which involves the reaction of an aldehyde group of mannose with free amine groups on the surface of SLN. This reaction forms Schiff's base (–N═CH–), which can be detected as a peak at approximately 1561.8 cm^{-1}. Therefore, the above-described results confirmed that the mannose surface modification on RIF-SLNs was successful.

To confirm that the Man-RIF SLNs contributed to the controlled release of rifampicin, the release rates of free rifampicin and Man-RIF SLNs were compared (Fig. 2B). Our findings indicated that 60% of the free rifampicin was released from the dialysis bag after 2 hours, reaching 90% in 5 hours. In contrast, approximately 30% of the Man-RIF SLNs were released after 2 hours, 70% at 5 hours, and 82% after 20 hours. The drug release experiments confirmed that the Man-RIF SLNs substantially slowed down the release of rifampicin, suggesting that they can greatly contribute to the sustained and long-term release of hydrophobic drugs.

Physical stability of Man-RIF SLNs

The stability of the Man-RIF SLNs was evaluated by measuring their average diameter, polydispersity index (PDI), and zeta potential. DLS measurements were performed using particles immediately after synthesis and after 9 months of cold storage (Fig. 2C). The average diameter of the initial particles was 195.7 ± 10.8 nm, whereas the size of the same particles after nine months decreased slightly to 179.8 ± 2.0 nm. However, this difference was not significant. PDI confirmed that both particles maintained a high dispersion of less than 0.2. The zeta potential of the particles immediately after synthesis was 32.2 ± 0.61 mV but decreased to 25.7 ± 1.9 mV after 9 months. Similar to the particle size, the zeta potential decreased slightly over time. However, these changes were not significant and the positive charge characteristics were maintained even after 9 months. Therefore, our stability tests confirmed that the particle size, dispersion, and zeta potential of the Man-RIF SLNs could be maintained for up to 9 months of storage.

In vitro cytotoxicity test

The MTT assay was performed to determine the cytotoxic effect of Man-RIF SLNs on M2 macrophages. First, the cytotoxicity of macrophages in response to rifampicin concentration was assessed to identify an appropriate treatment concentration. Fig. 3A shows the MTT assay results after treatment with free rifampicin at concentrations of 50, 100, 200, and 400 μg mL^{-1}. Cell viability remained above 85% up to the 100 μg mL^{-1}

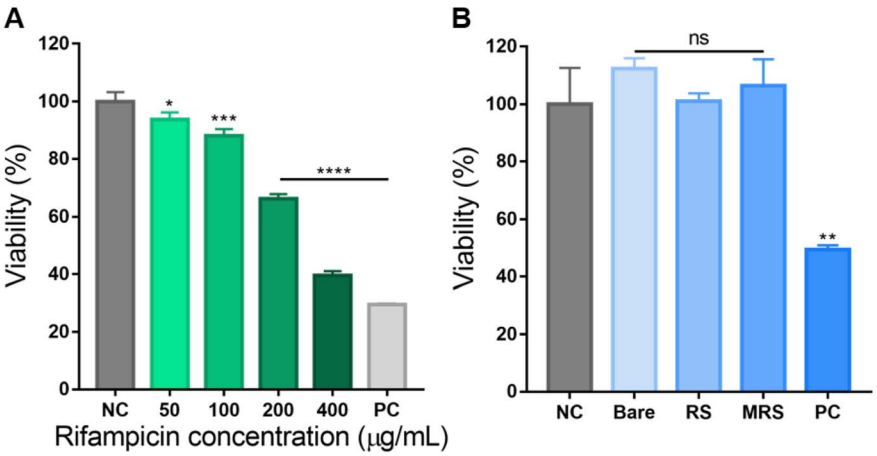

Fig. 3 (A) Cell cytotoxicity test on M2 macrophages depending on rifampicin concentration. (B) Cell cytotoxicity of bare SLNs, RIF-SLNs (RS), and Man-RIF SLNs (MRS) at a 100 μg mL^{-1} concentration on M2 macrophages. Non-significant values are represented as "ns"; *$p < 0.0332$, **$p < 0.0021$, ***$p < 0.0002$, ****$p < 0.0001$ *vs.* control.

concentration but then sharply decreased to below 66% at the 200 μg mL^{-1} concentration, which was indicative of cytotoxic effects. Therefore, all downstream experiments were conducted at a Man-RIF SLN concentration of 100 μg mL^{-1}. Fig. 3B shows the cytotoxicity of bare SLNs, RIF-SLNs, and Man-RIF SLNs after treatment at a concentration of 100 μg mL^{-1}, as determined by the MTT assay. When the viability of the negative control was set to 100% as a reference value, bare SLNs showed no significant cytotoxicity at 112.4%, and RIF-SLNs and Man-RIF SLNs also showed no significant cytotoxicity at 101.0 and 106.4%, respectively. Therefore, Man-RIF SLNs showed no significant cytotoxicity to immune cells and was confirmed to be a safe drug delivery vehicle.

Anti-biofilm and antibacterial test on *M.i.* cells

Many NTMs naturally form biofilms in many environments. Bacterial biofilms are microbial communities that are associated with chronic infections in humans. Biofilm formation inside the host protects the bacteria from the host immune system and increases resistance to antibiotics. In turn, this leads to recurrent infections or makes them more difficult to treat.[32] Therefore, anti-biofilm properties play an important role in the treatment of bacterial infectious diseases. To confirm the anti-biofilm effect of different treatment configurations, *M.i.* cells were treated with free rifampicin, Man-RIF SLNs, and RIF-SLNs at a 100 μg mL^{-1} concentration and then subjected to a crystal violet assay. When the biofilm removal effect of the positive control was assigned a value of 100% for reference, the biofilm inhibition rates of free rifampicin, Man-RIF SLNs, and RIF-SLNs were 87.0%, 79.0%, and 71.5% (Fig. 4A).

Next, a CFU assay was performed to confirm the antibacterial effect of Man-RIF SLNs on *M.i.* cells. The *M.i.* cells were treated with SLNs, RIF-SLNs, Man-RIF SLNs, and free rifampicin at a concentration of 100 μg mL^{-1}, and the antibacterial effect of these treatments was determined based on the number of bacterial colonies formed. The CFUs of each experimental group were measured as 100% of the CFUs of the negative control and analyzed based on this reference value. Fig. 4B shows the results of the CFUs formed in each of the experimental groups. The bare SLN treatment decreased CFU numbers by 15.5%. However, this antibacterial effect was not significant compared to the control. The RIF-SLN and Man-RIF SLN treatments decreased CFU numbers by 44.8 and 58.5%, respectively, indicating that particle conjugation enhanced the antibacterial effect of rifampicin. Free rifampicin showed the strongest antibacterial effect, with a 72.2% decrease in CFU numbers. However, although the free drug had the strongest antibacterial effect, it is important to note that the RIF-SLN and Man-RIF SLN treatments also had significant effects. Moreover, Man-RIF SLNs with mannose functionalization had superior anti-biofilm and antibacterial properties compared to RIF-SLNs.

Antibacterial test on *M.i.* inside macrophages

To confirm the antibacterial effect of Man-RIF SLNs on *M.i.* cells inside macrophages, macrophages were co-cultured with *M.i.* cells and a CFU assay was then conducted with the *M.i.* infected macrophages. PMA-differentiated M0 macrophages were infected with *M.i.* and treated with bare SLNs, RIF-SLNs, and Man-RIF SLNs at a concentration of 100 μg mL^{-1} for 24 hours. The macrophages were then lysed and the bacteria inside them were subjected to a CFU assay to compare the antibacterial effects of different treatments. Fig. 4C and D compare the CFU percentages of the experimental groups and the colonies formed on the plates, respectively. Based on the CFUs of the negative (untreated) control, the CFU of the bare SLN was 100.3%, which was not significantly different from the control. In contrast, the CFU percentage of the RIF-SLNs decreased to 73.3%, and the highest antibacterial effect was observed in the group treated with Man-RIF SLNs, with a CFU percentage of 36.0% relative to the control. Therefore, Man-RIF SLNs not only exhibited antibacterial effects against *M.i.* itself but also enhanced antibacterial effects against bacteria inside macrophages. Taken together, our results confirmed that cellular uptake and drug efficacy can be improved by delivering drugs through mannose-functionalized SLNs.

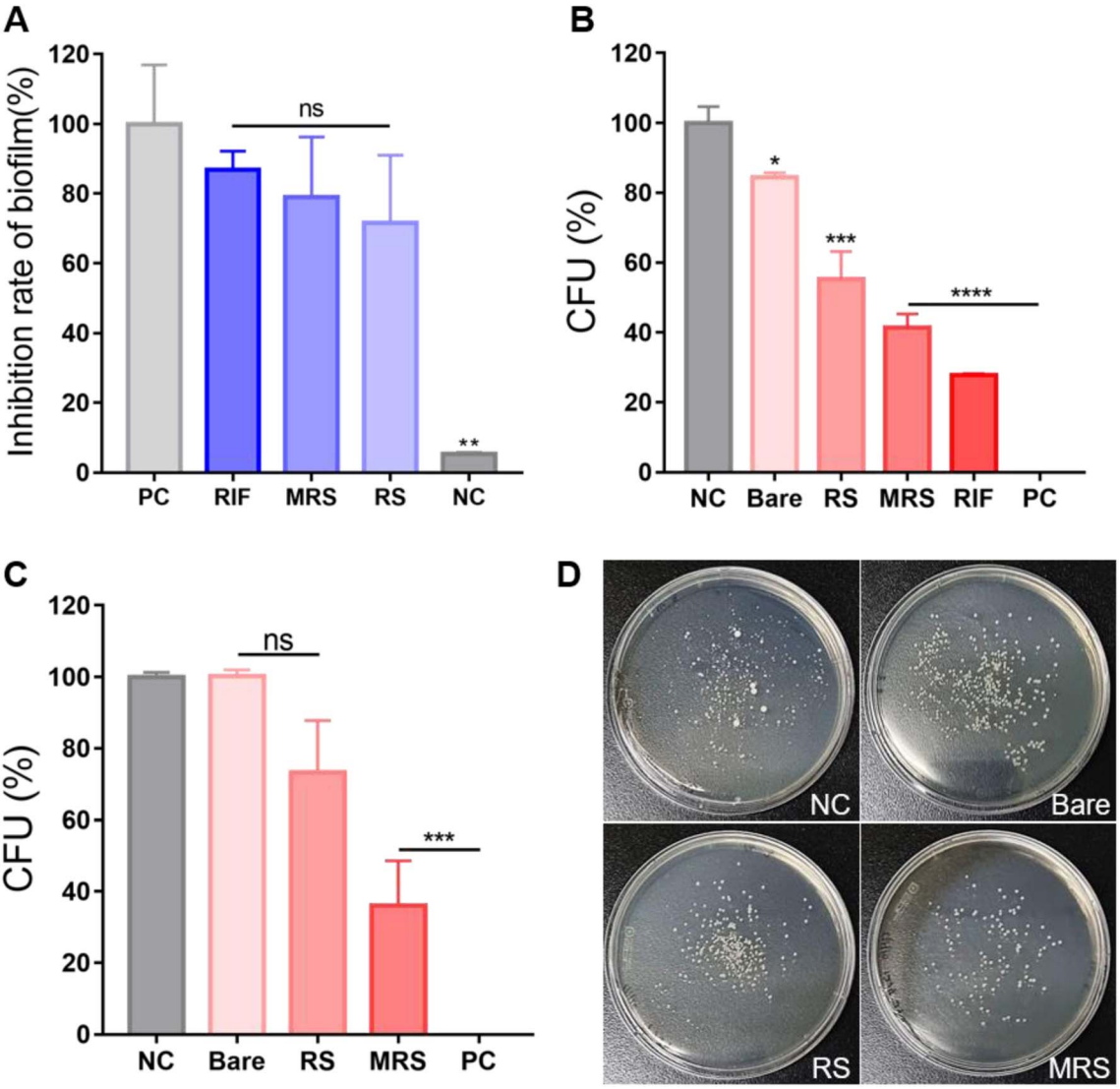

Fig. 4 (A) Crystal violet assay to confirm the anti-biofilm effect of Man-RIF SLNs. (B) Results of the colony forming unit (CFU) assay conducted with *M.i.* cells alone and (C) with *M.i.*-infected macrophages to confirm the antibacterial effect of Man-RIF SLNs. (D) Plate images of the formed bacterial colonies after conducting the CFU assay with bacterial cells extracted from infected macrophages. Non-significant values are represented as "ns"; *$p < 0.0332$, **$p < 0.0021$, ***$p < 0.0002$, ****$p < 0.0001$ *vs.* control.

Conclusion

The incidence of non-tuberculous lung diseases continues to rapidly increase worldwide, with MAC species being the most common pathogens. Once the bacteria begin to multiply and infect the lungs, they can lead to serious respiratory diseases such as bronchiectasis and chronic obstructive pulmonary disease. These infections are notoriously difficult to treat and conventional chemotherapy with multiple anti-TB drugs often leads to side effects due to long-term administration and increased drug resistance. To address this, we sought to improve drug delivery by targeting bacteria-infected macrophages. In this study, solid lipid nanoparticles (SLNs) were synthesized and loaded with the antituberculosis drug rifampicin (RIF) and the surface of the nanoparticles was modified with mannose to obtain mannose surface-modified RIF-SLNs (Man-RIF SLNs). The physical properties of the particles were then characterized to confirm that their surface had been successfully modified with mannose and our drug release experiments demonstrated that the Man-RIF SLNs controlled drug release and improved drug stability. Additionally, Man-RIF SLNs did not exert any observable cytotoxic effects on common immune cells and our experiments confirmed their antibacterial and anti-biofilm effects against *M.i.*, one of the causative agents of MAC. This study developed a targeted delivery system for rifampicin using solid lipid nanoparticles to reduce the side effects of prolonged antituberculosis treatment. Moreover, the Man-RIF SLNs synthesized herein exhibited significant antibacterial effects against *M.i.* cells. Collectively, our findings demonstrated that the synthesized Man-RIF SLNs are a promising drug delivery platform that not only enables the selective delivery of anti-TB

drugs to specific cells but also alleviates the side effects of existing therapies.

Author contributions

Yonghyun Choi, Shin Hyuk Kang and Jonghoon Choi supervised the study. Jayoung Chae, Jiwon Kim, Seung Hyun Kang, Suyeon Ahn and Younghyun Choi designed the study and performed the experiments. Jayoung Chae, Jiwon Kim, Seung Hyun Kang, Suyeon Ahn and Younghyun performed data analysis. Jayoung Chae, Yonghyun Choi, Shin Hyuk Kang and Jonghoon Choi wrote the manuscript.

Conflicts of interest

Dr Jonghoon Choi is the CEO/Founder, Dr Yonghyun Choi is the CTO, and Ms Jayoung Chae is the research associate of Feynman Institute of Technology at the Nanomedicine Corporation.

Acknowledgements

This work was supported by the National Research Foundation of Korea (NRF) grant funded by the Korean government (MSIT) (No. 2020R1A5A1018052, No. 2017M3A7B8061942, and No. 2019R1A2C1006018). This work was also supported by the Korea Environment Industry & Technology Institute (KEITI) funded by the Korea Ministry of Environment (MOE) (No. 2022002980003).

References

1 B. Banaschewski and T. Hofmann, Inhaled Antibiotics for Mycobacterial Lung Disease, *Pharmaceutics*, 2019, **11**(7), 352.
2 H. J. Kim, *et al.*, Role of ethambutol and rifampicin in the treatment of Mycobacterium avium complex pulmonary disease, *BMC Pulm. Med.*, 2019, **19**(1), 212.
3 K. Nakamura, *et al.*, Mycobacterium avium-intracellulare complex promote release of pro-inflammatory enzymes matrix metalloproteinases by inducing neutrophil extracellular trap formation, *Sci. Rep.*, 2022, **12**(1), 5181.
4 H. Parker, *et al.*, Mechanisms of Antibiotic Tolerance in Mycobacterium avium Complex: Lessons From Related Mycobacteria, *Front. Microbiol.*, 2020, **11**, 573983.
5 R. Diel, M. Lipman and W. Hoefsloot, High mortality in patients with Mycobacterium avium complex lung disease: a systematic review, *BMC Infect. Dis.*, 2018, **18**(1), 206.
6 V. Dartois and T. Dick, Drug development challenges in nontuberculous mycobacterial lung disease: TB to the rescue, *J. Exp. Med.*, 2022, **219**(6), e20220445.
7 B. S. Kwon, *et al.*, In Vitro MIC Values of Rifampin and Ethambutol and Treatment Outcome in Mycobacterium avium Complex Lung Disease, *Antimicrob. Agents Chemother.*, 2018, **62**(10), e00491.
8 Y. S. Kwon, W. J. Koh and C. L. Daley, Treatment of Mycobacterium avium Complex Pulmonary Disease, *Tuberc. Respir. Dis.*, 2019, **82**(1), 15–26.
9 T. Ozawa, *et al.*, Analysis of adverse drug events in pulmonary Mycobacterium avium complex disease using spontaneous reporting system, *BMC Infect. Dis.*, 2022, **22**(1), 580.
10 S. Kim, F. Masum and J. S. Jeon, Recent Developments of Chip-based Phenotypic Antibiotic Susceptibility Testing, *Biochip J.*, 2019, **13**(1), 43–52.
11 S. W. Pan, *et al.*, Treatment for Mycobacterium avium complex lung disease, *J. Formosan Med. Assoc.*, 2020, **119**(1), S67–S75.
12 H. Kim, *et al.*, Multiplex Molecular Point-of-Care Test for Syndromic Infectious Diseases, *BioChip J.*, 2021, **15**(1), 14–22.
13 H.-Y. Jeon, A.-J. Lee and K.-S. Ha, Polymer-Based Delivery of Peptide Drugs to Treat Diabetes: Normalizing Hyperglycemia and Preventing Diabetic Complications, *BioChip J.*, 2022, **16**(2), 111–127.
14 B. Kang, *et al.*, Magnetic Nanochain-Based Smart Drug Delivery System with Remote Tunable Drug Release by a Magnetic Field, *BioChip J.*, 2022, **16**(3), 280–290.
15 Y. Ha and I. Kim, Recent Developments in Innovative Magnetic Nanoparticles-Based Immunoassays: From Improvement of Conventional Immunoassays to Diagnosis of COVID-19, *BioChip J.*, 2022, **16**(4), 351–365.
16 S. Parvez, *et al.*, Modified solid lipid nanoparticles encapsulated with Amphotericin B and Paromomycin: an effective oral combination against experimental murine visceral leishmaniasis, *Sci. Rep.*, 2020, **10**(1), 12243.
17 P. K. Sahu, *et al.*, Mannosylated solid lipid nanoparticles for lung-targeted delivery of Paclitaxel, *Drug Dev. Ind. Pharm.*, 2015, **41**(4), 640–649.
18 M. J. Mitchell, *et al.*, Engineering precision nanoparticles for drug delivery, *Nat. Rev. Drug Discovery*, 2021, **20**(2), 101–124.
19 N. Dhiman, *et al.*, Lipid Nanoparticles as Carriers for Bioactive Delivery, *Front. Chem.*, 2021, **9**, 580118.
20 M. J. Byun, *et al.*, Advances in Nanoparticles for Effective Delivery of RNA Therapeutics, *BioChip J.*, 2022, **16**(2), 128–145.
21 S. Scioli Montoto, G. Muraca and M. E. Ruiz, Solid Lipid Nanoparticles for Drug Delivery: Pharmacological and Biopharmaceutical Aspects, *Front. Mol. Biosci.*, 2020, **7**, 587997.
22 E. Rostami, *et al.*, Drug targeting using solid lipid nanoparticles, *Chem. Phys. Lipids*, 2014, **181**, 56–61.
23 M. K. Shin and S. J. Shin, Genetic Involvement of Mycobacterium avium Complex in the Regulation and Manipulation of Innate Immune Functions of Host Cells, *Int. J. Mol. Sci.*, 2021, **22**(6).
24 Y. Zhang, *et al.*, Separation of Macrophages Using a Dielectrophoresis-Based Microfluidic Device, *BioChip J.*, 2020, **14**(2), 185–194.
25 E. C. Patin, S. J. Orr and U. E. Schaible, Macrophage Inducible C-Type Lectin As a Multifunctional Player in Immunity, *Front. Immunol.*, 2017, **8**, 861.
26 Y. Choi, *et al.*, Surface glycan targeting for cancer nanoimmunotherapy, *J. Contr. Release*, 2022, **342**, 321–336.
27 Y. Choi, *et al.*, Glycan targeting nanoparticle for photodynamic immunotherapy of melanoma, *Acta Pharm. Sin. B*, 2023, **13**(5), 1903–1918.

28 E. Dalle Vedove, G. Costabile and O. M. Merkel, Mannose and Mannose-6-Phosphate Receptor-Targeted Drug Delivery Systems and Their Application in Cancer Therapy, *Adv. Healthcare Mater.*, 2018, **7**(14), e1701398.
29 R. Goswami, *et al.*, Mannosylation of LNP Results in Improved Potency for Self-Amplifying RNA (SAM) Vaccines, *ACS Infect. Dis.*, 2019, **5**(9), 1546–1558.
30 D. Strassburger, *et al.*, Mannose-Decorated Multicomponent Supramolecular Polymers Trigger Effective Uptake into Antigen-Presenting Cells, *Chembiochem*, 2018, **19**(9), 912–916.
31 N. Nimje, *et al.*, Mannosylated nanoparticulate carriers of rifabutin for alveolar targeting, *J. Drug Targeting*, 2009, **17**(10), 777–787.
32 P. Chakraborty, *et al.*, Biofilm formation in the lung contributes to virulence and drug tolerance of Mycobacterium tuberculosis, *Nat. Commun.*, 2021, **12**(1), 1606.